Received: 12 April 2018 | Revised: 19 July 2018 | Accepted: 5 September 2018

DOI: 10.4218/etrij.2018-0190

ORIGINAL ARTICLE

WILEY ETRI Journal

Computationally efficient variational Bayesian method for PAPR reduction in multiuser MIMO-OFDM systems

Davinder Singh | **Rakesh Kumar Sarin**

Department of Electronics and Communication Engineering, Dr. B.R. Ambedkar National Institute of Technology, Jalandhar, Punjab, India

Correspondence
Davinder Singh, Department of Electronics and Communication Engineering, Dr. B.R. Ambedkar National Institute of Technology, Jalandhar, Punjab, India.
Email: davinders.15.phd@nitj.ac.in

This paper investigates the use of the inverse-free sparse Bayesian learning (SBL) approach for peak-to-average power ratio (PAPR) reduction in orthogonal frequency-division multiplexing (OFDM)-based multiuser massive multiple-input multiple-output (MIMO) systems. The Bayesian inference method employs a truncated Gaussian mixture prior for the sought-after low-PAPR signal. To learn the prior signal, associated hyperparameters and underlying statistical parameters, we use the variational expectation-maximization (EM) iterative algorithm. The matrix inversion involved in the expectation step (E-step) is averted by invoking a relaxed evidence lower bound (relaxed-ELBO). The resulting inverse-free SBL algorithm has a much lower complexity than the standard SBL algorithm. Numerical experiments confirm the substantial improvement over existing methods in terms of PAPR reduction for different MIMO configurations.

KEYWORDS
multiuser MIMO-OFDM, PAPR reduction, sparse Bayesian leaning (SBL)

1 | INTRODUCTION

Since its inception in 2010 by Marzetta [1], massive multiple-input multiple-output (MIMO) systems have emerged as a potential technology to achieve significant improvements with respect to the spectral and energy efficiency of wireless communication systems. Unlike traditional small-scale MIMO systems, very large-scale multiuser MIMO or massive MIMO systems employ base station (BS) antenna arrays with several hundred antennas to simultaneously serve multiple single-antenna terminals over the same time-frequency resource. As with most propagation environments, the large number of transmit antennas at the BS results in favorable propagation; hence, simple linear processing becomes nearly optimal. Moreover, the occurrence of the "channel hardening" phenomenon averages out the impact of small-scale fading, which simplifies the complexity of the scheduling scheme [2]. Despite these many benefits, massive MIMO systems face many practical challenges to their successful commercial deployment [3].

In practice, MIMO technology is integrated into orthogonal frequency-division multiplexing (OFDM), which is a multicarrier modulation technique designed to mitigate against frequency-selective fading. However, the disadvantage of OFDM-based transmission systems is their high peak-to-average power ratio (PAPR) because many subcarriers are combined via an inverse fast Fourier transform (IFFT) operation [4]. In OFDM implementations of massive MIMO systems, the problem of high PAPR is more pronounced as the number of transmit antennas is increased. Eventually, the installation of highly linear, but expensive power amplifiers at the front end of BSs will significantly increase the hardware cost as well as the power consumption. Thus, the practical implementation of massive MIMO requires the use of non-linear and power-efficient power amplifiers. Therefore, signals with low-PAPR values are critical to enabling the use of affordable and power-efficient power amplifiers for multiuser massive MIMO systems.

Several schemes, such as precoding [5], clipping [6], partial transmit sequence (PTS) [7], tone reservation (TR) [8], selected mapping (SLM) [9], and active constellation extension (ACE) [10] have been proposed to address the high PAPR in single-input single-output (SISO) OFDM systems. Most of these techniques have been successfully analyzed for single-user (SU) multi-antenna systems [11–14]. However, these are not easily applicable to multi-user (MU) MIMO systems because unlike the point-to-point case, the joint processing of the signals is only feasible at the transmitter end as the user terminals are spatially distributed. In massive MIMO, the inherent degrees-of-freedom (DoFs) can be conveniently utilized for PAPR reduction. The proposed precoding-based PAPR reduction method in [15] exploits the null spaces of massive MU-MIMO-OFDM channels based on a linear constrained l optimization problem. The convex optimization via fast iterative truncation algorithm (FITRA) jointly considers the PAPR reduction and MU interference (MUI) suppression.

In addition to the above-mentioned techniques, the PAPR reduction achieved in SISO systems using compressed sensing [16] has also been reported in literature, for example, [17] and [18]. Among the compressed sensing techniques, sparse Bayesian learning (SBL) [19] has attracted much attention over greedy methods, for example, the orthogonal matching pursuit [20] and the basis pursuit (BP) method [21]. Although SBL outperforms the greedy pursuit strategies and the basis pursuit (BP) method, its major drawback is that for a $J \times K$ ($J \ll K$) sampling matrix, it requires the computation of the inverse of a $K \times K$ matrix at each iteration. The computational complexity (of order $[K^3]$) thus grows exponentially with the problem size. To alleviate this problem, in [22], generalized approximate message passing (GAMP) was embedded in the variational expectation-maximization (EM) framework in order to obtain approximate marginal posteriors with a much lower computational complexity (of order $\mathcal{O}$ $[J,K]$). The variational EM-GAMP framework was employed to solve a variety of compressed sensing problems, for example, [23] and [24], as well as the PAPR reduction problem [25]. Recently, a computationally efficient SBL method was developed in [26], and it successfully replaced the costly matrix-inversion operation of the conventional EM-based implementation of SBL.

In this study, we developed an inverse-free SBL method to jointly consider the PAPR reduction and MUI cancellation problem for MU OFDM-based large-scale MIMO systems by resorting to the method proposed in [26]. To seek a low-PAPR solution, the two-layered hierarchical modeling places a truncated Gaussian-inverse-Gamma prior on the unknown signal (that is, the solution). We resort to the EM algorithm to learn the prior signal, associated hyperparameters, and other underlying statistical parameters. The matrix inversion involved in the traditional implementation of SBL is prevented by invoking a relaxed evidence lower bound (relaxed-ELBO), which is then maximized using the EM scheme, resulting in an inverse-free SBL approach. Thus, the resulting algorithm does not require the use of GAMP to circumvent the matrix-inverse operation. The simulation results reveal that the proposed method is superior to the existing methods in terms of PAPR reduction and computational complexity.

The remainder of the paper is organized as follows: Section 2 presents a description of the system model, basic assumptions, and introduction to the PAPR reduction problem. Then, a two-layered truncated Gaussian-inverse-Gamma prior model is presented in Section 3. Section 4 provides a brief review of variational Bayesian inference, and describes the development of an inverse-free Bayesian inference approach. In Section 5, simulation results are presented to compare the performance with existing methods, and conclusions are given in section 6.

Notation: Throughout the paper, lowercase and uppercase symbols such as "$\mathbf{x}$" and "$\mathbf{X}$" are used to represent column vectors and matrices, respectively, and we use $(\mathbf{X})^{\mathrm{T}}$, $(\mathbf{X})^{\mathrm{H}}$, and tr $(\mathbf{X})$ to denote the transpose, conjugate transpose, and trace, respectively. The inner product of two vectors $\mathbf{x}$ and $\mathbf{y}$ is represented as $<\mathbf{x}, \mathbf{y}> = \mathbf{x}^{\mathrm{T}}\mathbf{y}$. Moreover $\|\mathbf{x}\|_1$, $\|\mathbf{x}\|_2$ and $\|\mathbf{x}\|_\infty$ are used to denote the l_1-norm, l_2-norm, and l_∞-norm of a vector $\mathbf{x}$. $\Re\{\mathbf{x}$ and $\Im\{\mathbf{x}\}$, respectively represent the real and imaginary parts of vector $\mathbf{x}$. The $U \times U$ unitary discrete Fourier transform is represented by $\mathbf{F}_U$. The $N \times N$ identity matrix and $M \times N$ zero matrix are represented as $\mathbf{I}_N$ and $0_{M\times N}$, respectively. The symbol $\otimes$ represents the Kronecker product. We use $p(x)$ to denote the probability distribution function (pdf) of a random quantity x, and $N(\boldsymbol{x}; m, v)$ to denote the Gaussian pdf with mean x and variance v.

2 | SYSTEM DESCRIPTION AND PROBLEM FORMULATION

2.1 | System model

Consider the downlink transmission of a massive MU MIMO system depicted in Figure 1, where the BS having N transmit antennas communicates with M ($\ll N$) single-antenna equipped terminals. For a total of U OFDM tones (subcarriers), the transmitted signal vector $\mathbf{s}_u \in \mathcal{O}^{M\times 1}$ contains information at the uth tone intended for the M terminals. The subcarriers are partitioned into two complementary sets Γ and Γ^{C}. The set Γ contains data transmission tones, whereas the complementary set Γ^{C} indexes the inactive guard-band tones located at the edges of the spectrum, such that for each tone, $u \in \Gamma^{\mathrm{C}}$ $\mathbf{s}_u = 0_{M\times 1}$.

To eliminate the MUI at the receivers, it is assumed that the BS has perfect knowledge of channel matrices $\mathbf{H}_u \in$

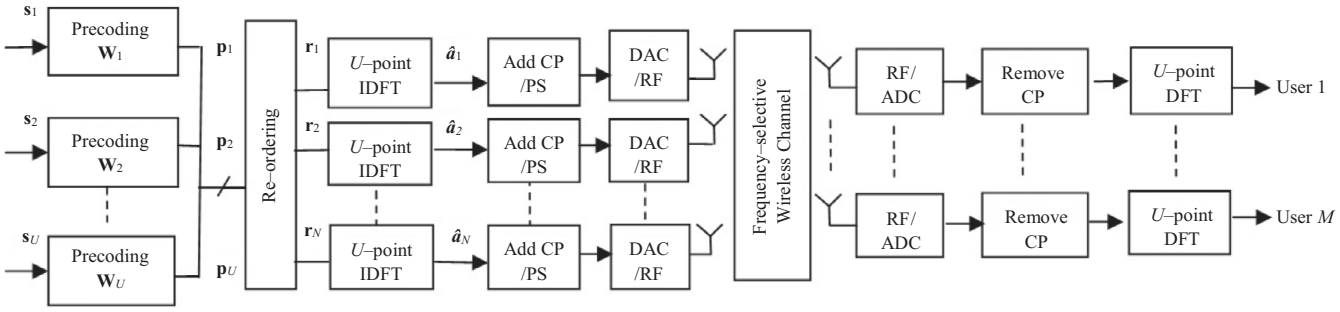

FIGURE 1 Massive multiuser MIMO-OFDM downlink scenario, with U OFDM tones, N transmit antennas, and M user-terminals

$\mathbf{C}^{M\times N}$ so that the information symbols on the uth subcarrier are linearly precoded as

$$\mathbf{p}_u = \mathbf{W}_u \mathbf{s}_u, \tag{1}$$

where $\mathbf{p}_u = \mathbf{C}^{N\times 1}$ is the precoded vector and $\mathbf{W}_u = \mathbf{C}^{N\times M}$ represents the precoding matrix for the uth OFDM tone. The prominent linear precoding schemes for massive MIMO are maximum ratio transmission (MRT), zero-forcing (ZF), and minimum mean-square error (MMSE) precoding [27]. To cancel out the MUI at each user, we consider the ZF precoding scheme, which implements a pseudo-inverse of the channel matrix $\mathbf{H}$, that is,

$$\mathbf{W}_u^{\mathrm{ZF}} \propto \mathbf{H}_u^{\mathrm{H}} (\mathbf{H}_u \mathbf{H}_u^{\mathrm{H}})^{-1}. \tag{2}$$

After precoding, the normalized precoded vectors $\mathbf{p}_u$, $\forall u$ are then reordered to N transmit antennas for OFDM modulation according to the following mapping:

$$[\mathbf{r}_1, \mathbf{r}_2, \ldots, \mathbf{r}_N] = [\mathbf{p}_1, \mathbf{p}_2, \ldots, \mathbf{p}_U]^{\mathrm{T}}, \tag{3}$$

where the U-dimensional vector $\mathbf{r}_n$ contains the frequency-domain signal to be transmitted from the nth antenna.

Then, an inverse discrete Fourier transform (IDFT) $\mathbf{F}$ is applied on the precoded signal to obtain the time-domain signal, that is,

$$\hat{\mathbf{a}}_n = \mathbf{F}_U^{\mathrm{H}} \boldsymbol{r}_n, \tag{4}$$

The IDFT operation is followed by the insertion of the cyclic prefix into the time-domain samples of each antenna in order to eliminate intersymbol interference (ISI). Finally, the time-domain samples are upconverted and transmitted through the frequency-selective channel.

At the receivers, after the removal of the cyclic prefixes, the frequency-domain signal is obtained by performing a discrete Fourier transform (DFT). The signal received by M user terminals can be described as

$$\mathbf{f}_u = \mathbf{H}_u \mathbf{p}_u + \mathbf{e}_u, \tag{5}$$

where $\mathbf{f}_u \in \mathbf{C}^{M\times 1}$ is the received vector associated with the uth tone, and $\mathbf{e}_u \in \mathbf{C}^{M\times 1}$ denotes the independent and identically distributed (i.i.d.) complex Gaussian receiver noise, and has entries with zero mean and variance N_{o}. If ZF precoding is employed, transmitting $\mathbf{p}_u = \mathbf{H}_u^{\mathrm{H}} (\mathbf{H}_u \mathbf{H}_u^{\mathrm{H}})^{-1} \mathbf{s}_u$ perfectly eliminates all MUI, that is, it transforms (5) into M independent single-stream systems $\mathbf{f}_u = \mathbf{s}_u + \mathbf{e}_u \ \forall_u$.

2.2 | Peak-to-average power ratio (PAPR) aware precoding

The time-domain samples $\{\hat{\boldsymbol{a}}_n\}$ exhibit a high dynamic range owing to the superposition of the individual subcarriers, which when transmitted through a non-linear power amplifier, suffer in-band distortion and generate undesired out-of-band radiation. This requires the use of power-inefficient and expensive linear power amplifiers. The large dynamic range of the OFDM-modulated signals on the nth antenna can be characterized by the PAPR metric as [28]:

$$\mathrm{PAPR}_n = \frac{2U \|\hat{\boldsymbol{a}}_n\|_{\tilde{\infty}}^2}{\|\hat{\boldsymbol{a}}_n\|_2^2}. \tag{6}$$

where the $\boldsymbol{l}_{\tilde{\infty}}$-norm is defined as $\|\hat{\boldsymbol{a}}_n\|_{\tilde{\infty}} = \max\{\Re\|\hat{\boldsymbol{a}}_n\|_\infty, \Im\|\hat{\boldsymbol{a}}_n\|_\infty\}$. The operator $\|.\|_{\tilde{\infty}}^2$ is used, because RF-chain implementations process and modulate the real and imaginary parts independently. However, minimizing the PAPR as defined in (6) also ensures an l_∞-norm-based PAPR reduction.

The best- and worst-case PAPR are bounded as

$$1 \le \mathrm{PAPR}_n \le 2U. \tag{7}$$

Because the transmit antennas are greater in number than user terminals, that is, $N \gg M$, this implies that there will generally be an infinitely large number of precoded signals, $\mathbf{p} \triangleq [\mathbf{p}_1^{\mathrm{T}}, \mathbf{p}_2^{\mathrm{T}}, \ldots, \mathbf{p}_U^{\mathrm{T}}]^{\mathrm{T}}$ satisfying the precoding constraint $\mathbf{s} = \mathbf{H}\mathbf{p}$. Thus, we aim to search for the precoded signal $\mathbf{p}$ whose associated time-domain signals $\{\hat{\boldsymbol{a}}_n\}$ result in a small dynamic range, while obeying the following conditions to cancel out the MUI.

$$\begin{cases} \mathbf{s}_u = \mathbf{H}_u \mathbf{p}_u, & u \in \Gamma, \\ \mathbf{0}_{N\times 1} = \mathbf{p}_u, & u \in \Gamma^{\mathrm{C}}. \end{cases} \equiv \bar{\mathbf{s}} = \bar{\mathbf{H}}\mathbf{p} \tag{8}$$

where $\bar{\mathbf{s}} \in \mathbf{C}^{UM\times 1}$ is the aggregation of all user data symbols and nulls on guard-band frequencies, and $\bar{\mathbf{H}}$ corresponds to a block diagonal matrix having the main diagonal blocks as $\mathbf{H}_u$, $\forall u \in \Gamma$ and $\mathbf{I}_N$, $\forall u \in \Gamma^{\mathrm{C}}$.

As defined in (3), the entries of each precoded vector are assigned to N transmit antennas through a linear transformation $\boldsymbol{T}$ as:

$$\mathbf{r} = \boldsymbol{T}\mathbf{p}, \tag{9}$$

Using (4) and (8), the constraints on no MUI and no energy in the guard bands can be obtained as

$$\bar{\mathbf{s}} = \bar{\mathbf{H}}\boldsymbol{T}^{\mathrm{T}}\bar{\mathbf{F}}\hat{\boldsymbol{a}} \tag{10}$$

where $\bar{\mathbf{F}} \triangleq \mathbf{I}_N \otimes \mathbf{F}_U$ and $\hat{\boldsymbol{a}} \triangleq \left[\hat{\boldsymbol{a}}_1^{\mathrm{T}}, \hat{\boldsymbol{a}}_2^{\mathrm{T}}, \ldots, \hat{\boldsymbol{a}}_N^{\mathrm{T}}\right]^{\mathrm{T}}$.

For symbol vector $\bar{\mathbf{s}}$, the aim was to find the time-domain samples $\hat{\boldsymbol{a}}$ that satisfy (10) such that each antenna emits signals with low PAPR. As indicated in [15], the PAPR minimax reduction problem can be framed as a constrained optimization that reduces the $l_{\tilde{\infty}}$-norm of the aggregated time-domain vector $\hat{\boldsymbol{a}}$.

$$\min\|\hat{\boldsymbol{a}}\|_{\tilde{\infty}} \text{ subject to } \bar{\mathbf{s}} = \bar{\mathbf{H}}\boldsymbol{T}^{\mathrm{T}}\bar{\mathbf{F}}\hat{\boldsymbol{a}}. \tag{11}$$

Here, all time-domain symbols $\{\hat{\boldsymbol{a}}_n\}$ are stacked in vector $\hat{\boldsymbol{a}}$.

Eventually, the above problem can be transformed into an equivalent real-valued l_∞-norm-based problem as follows

$$\min_x \|\mathbf{x}\|_\infty \text{ s.t. } \mathbf{y} = \mathbf{H}\mathbf{x} \tag{12}$$

where $\mathbf{y} \triangleq \begin{bmatrix} \Re\{\bar{\mathbf{s}}\} \\ \Im\{\bar{\mathbf{s}}\} \end{bmatrix}$, $\mathbf{x} \triangleq \begin{bmatrix} \Re\{\hat{\boldsymbol{a}}\} \\ \Im\{\hat{\boldsymbol{a}}\} \end{bmatrix}$ and

$$\bar{\mathbf{H}} \triangleq \begin{bmatrix} \Re\{\bar{\mathbf{H}}\boldsymbol{T}^{\mathrm{T}}\bar{\mathbf{F}}\} & -\Im\{\bar{\mathbf{H}}\boldsymbol{T}^{\mathrm{T}}\bar{\mathbf{F}}\} \\ \Im\{\bar{\mathbf{H}}\boldsymbol{T}^{\mathrm{T}}\bar{\mathbf{F}}\} & \Re\{\bar{\mathbf{H}}\boldsymbol{T}^{\mathrm{T}}\bar{\mathbf{F}}\} \end{bmatrix}_{2\left(|\varphi|M+\left|\varphi^C\right|N\right)\times 2UN}.$$

To facilitate the development of the FITRA [15], in order to minimize the largest magnitude of all antennas' signals, (12) can be restated in Lagrangian form as

$$\min_x \lambda\|\mathbf{x}\|_\infty + \|\mathbf{y} - \mathbf{H}\mathbf{x}\|_2^2, \tag{13}$$

where λ is a suitably chosen non-zero positive regularization parameter that serves as a tradeoff between the PAPR minimization and data-fitting error.

3 | SPARSE BAYESIAN LEARNING FRAMEWORK FOR PAPR REDUCTION

To frame the PAPR reduction as a sparse signal-recovery problem, the equality constraint in (12) can be relaxed to the following form

$$\mathbf{y} = \mathbf{H}\mathbf{x} + \delta \tag{14}$$

where the additive noise term δ models the mismatch between $\mathbf{y}$ and $\mathbf{H}\mathbf{x}$, and is assumed to be mean-zero Gaussian with variance $\beta = 1/\sigma^2$, that is, $p(\beta) = N\left(\delta\middle|0, \beta^{-1}\mathbf{I}\right)$.

Inspired by [25], our objective is to seek a quasi-constant magnitude solution to the linear inverse problem (14) whose maximally possible entries fall on the boundary, and the remainder lie within the specified interval $[-v, v]$ in order to satisfy the MUI cancellation constraint. In the first layer of the two-layered hierarchical prior, we assume that the coefficients of $\boldsymbol{x}$ are mutually independent such that each entry $\boldsymbol{x}_i$ satisfies

$$p(x_i) = \begin{cases} \pi\frac{\mathrm{N}(\boldsymbol{x}_i; v, \alpha_{i1}^{-1})}{\eta_{i1}} + (1-\pi)\frac{\mathrm{N}(\boldsymbol{x}_i; -v, \alpha_{i2}^{-1})}{\eta_{i2}} & \text{if } \boldsymbol{x}_i \in [-v, v], \\ 0, & \text{otherwise} \end{cases} \tag{15}$$

which is called a truncated Gaussian prior distribution lying within the interval $[-v, v]$. Each Gaussian density is called a component of the Gaussian mixture model such that the first component has its own mean v and variance α_{i1}^{-1}, and the second component is characterized by mean $-v$ and variance α_{i2}^{-1}. Here, the mixing coefficient $\pi \in [0, 1]$ denotes the percentage of each component. The normalization constant η_{il} of the lth component is given by

$$\eta_{i1} = 0.5 - \varphi\left(-2v\sqrt{\alpha_{i1}^{-1}}\right), \eta_{i2} = \varphi\left(2v\sqrt{\alpha_{i2}^{-1}}\right) - 0.5. \tag{16}$$

Following the conventional SBL framework [19], the precision parameters $\boldsymbol{\alpha}_1 = \{\alpha_{i1}\}_{i=1}^I$ and $\boldsymbol{\alpha}_2 = \{\alpha_{i2}\}_{i=1}^I$ are imposed by their conjugate hyperprior, that is, the Gamma distribution with respect to parameters a and b in the second layer.

$$p(\boldsymbol{\alpha}_1\boldsymbol{\alpha}_2; a, b) = \prod_{l=1}^{2}\prod_{i=1}^{K}\mathrm{Gamma}(\alpha_{li}|a, b), \tag{17}$$

where

$$\mathrm{Gamma}(\alpha|\boldsymbol{a}, \boldsymbol{b}) = \Gamma(\boldsymbol{a})^{-1}\boldsymbol{b}^{\boldsymbol{a}}\alpha^{\boldsymbol{a}-1}\boldsymbol{e}^{-\boldsymbol{b}\alpha} \tag{18}$$

with $\Gamma(a) = \int_0^\infty t^{a-1}e^{-t}dt$, the *gamma* function.

Moreover, a Gamma hyperprior is placed over β to learn the inverse of the noise variance β, that is,

$$p(\beta; c, d) = \mathrm{Gamma}(\beta|c, d) = \Gamma(c)^{-1}d^c\beta^{c-1}e^{-d\beta}. \tag{19}$$

The parameters a, b, c, and d are set to small values, for example, $a = b = c = d = 10^{-10}$ in order to make these priors non-informative. Generally, the Bayesian inference algorithm needs to compute the logarithm of the prior; however, (15) is an intractable form. Therefore, we introduce a binary hidden variable $\boldsymbol{\kappa}_i$ in order to transform the prior into an exponential close-form. The equivalent distribution of $\boldsymbol{x}_i$ can be written as

$$p(x_i|\alpha_{i1}, \alpha_{i2}, \kappa_i; v) = \left\{\left(\frac{\mathrm{N}(\boldsymbol{x}_i; v, \alpha_{i1}^{-1})}{\eta_{i1}}\right)^{\kappa_i}\left(\frac{\mathrm{N}(\boldsymbol{x}_i; -v, \alpha_{i2}^{-1})}{\eta_{i2}}\right)^{1-\kappa_i}, \boldsymbol{x}_i \in [-v, v], \right. \tag{20}$$

where the distribution for the latent variable κ_i is

$$p(\kappa_i; \pi) = (\pi)^{\kappa_i}(1-\pi)^{1-\kappa_i}. \tag{21}$$

The resultant hierarchical graphical model for low-PAPR signal priors is shown in Figure 2.

3.1 | Variational Bayesian inference

In the hierarchical model shown in Figure 2, $\theta = \{\boldsymbol{x}, \boldsymbol{\alpha_1}, \boldsymbol{\alpha}_2, \beta, \boldsymbol{\kappa}\}$ denote the hidden variables such that the variational distribution is expressed as $q(\boldsymbol{\theta}) = q(\boldsymbol{x})q(\alpha_1)q(\alpha_2)q(\beta)q(\kappa)$. Before updating the hyperparameters, we will provide a brief review of the iterative EM algorithm [29].

3.1.1 | Overview of variational inference

We denote $\boldsymbol{y}$ as the observed data, θ as the hidden variables, and $\boldsymbol{\Theta} = \{v, z\}$ as the unknown deterministic parameters in the hierarchical model. The log-likelihood of the observed data can be written as

$$\ln p(\boldsymbol{y}; \boldsymbol{\Theta}) = L(q, \boldsymbol{\Theta}) + \mathrm{KL}(q\|p), \tag{22}$$

with

$$\begin{aligned} L(q, \Theta) &= \int q(\boldsymbol{\theta}) \ln\left(\frac{p(\boldsymbol{y}, \boldsymbol{\theta}; \Theta)}{q(\boldsymbol{\theta})}\right) d\boldsymbol{\theta} \\ \mathrm{KL}(q\|p) &= -\int q(\boldsymbol{\theta}) \ln\left(\frac{p(\boldsymbol{\theta}|\boldsymbol{y}; \Theta)}{q(\boldsymbol{\theta})}\right) d\boldsymbol{\theta} \end{aligned} \tag{23}$$

where $\mathrm{KL}(q\|p) \geq 0$ is the Kullback-Leibler divergence between the posterior distribution $p(\boldsymbol{\theta}|\boldsymbol{y}; \Theta)$ and variational distribution $q(\boldsymbol{\theta})$, and $L(q, \Theta)$ is the ELBO of the log-likelihood $\ln p(\boldsymbol{y}; \Theta)$. Clearly, the equality holds only if $\mathrm{KL}(q\|p) = 0$, that is, $p(\boldsymbol{\theta}|\boldsymbol{y}; \Theta) = q(\boldsymbol{\theta})$. The EM algorithm iteratively maximizes the ELBO $L(q, \Theta)$ over $q(\boldsymbol{\theta})$ and Θ.

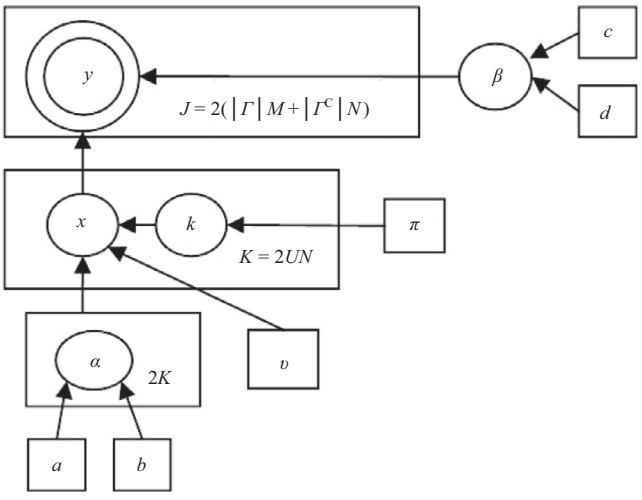

FIGURE 2 Graphical model for signal priors, with circles, double circles, and squares representing hidden variables, observed variables, and model parameters, respectively

The ELBO can be re-expressed as

$$L(q, \Theta) = \int q(\boldsymbol{\theta}) \ln \frac{p(\boldsymbol{y}|\boldsymbol{x}, \beta) p(\boldsymbol{x}|\alpha_1, \alpha_2, \kappa; v) p(\alpha_1) p(\alpha_2) p(\beta) p(\kappa)}{q(\boldsymbol{\theta})} d\boldsymbol{\theta} \tag{24}$$

Because the variables $\{\boldsymbol{x}_i\}$ in $p(\boldsymbol{y}|\boldsymbol{x}, \beta)$ are non-factorizable, updating the approximate posterior distribution $q(\boldsymbol{x})$ becomes intractable. The high computational cost involved in obtaining $q(\boldsymbol{x})$ owing to the computation of the inverse of a $K \times K$ matrix at each iteration inhibits the application of the conventional SBL method. In order to circumvent the matrix-inverse operation, [26] found a relaxed-ELBO, that is, a lower bound on $L(q)$. With respect to the lower bound on $p(\boldsymbol{y}|\boldsymbol{x}, \beta)$, from [26], we obtain the following inequality

$$\begin{aligned} p(\boldsymbol{y}|\boldsymbol{x}, \beta) &= \frac{\beta^{J/2}}{\sqrt{2\pi}} \exp\left(-\frac{\beta}{2}\|\boldsymbol{y} - \mathbf{H}\boldsymbol{x}\|_2^2\right) \\ &\geq \frac{\beta^{J/2}}{\sqrt{2\pi}} \exp\left(-\frac{\beta}{2}\boldsymbol{g}(\boldsymbol{x}, z)\right) = \mathbf{F}(\boldsymbol{y}, \boldsymbol{x}, z, \beta) \end{aligned} \tag{25}$$

where

$$\boldsymbol{g}(\boldsymbol{x}, z) = \|\boldsymbol{y} - \mathbf{H}\boldsymbol{z}\|_2^2 + 2(\boldsymbol{x} - \boldsymbol{y})^{\mathrm{T}}\mathbf{H}^{\mathrm{T}}(\mathbf{H}\boldsymbol{z} - \boldsymbol{y}) + \frac{T}{2}\|\boldsymbol{x} - \boldsymbol{z}\|_2^2 \tag{26}$$

for Lipschitz constant T.

Substituting (24) into (23), a relaxed-ELBO can be obtained as

$$L(q) \geq \tilde{L}(q, \Theta) = \int q(\boldsymbol{\theta}) \ln \frac{G(\boldsymbol{y}, \boldsymbol{\theta}, \boldsymbol{\Theta})}{q(\boldsymbol{\theta})} d\boldsymbol{\theta} \tag{27}$$

where

$$\boldsymbol{G}(\boldsymbol{y}, \theta, \boldsymbol{\Theta}) = F(\boldsymbol{y}, \boldsymbol{x}, z, \beta) p(\boldsymbol{x}|\alpha_1, \alpha_2, \kappa; v) p(\alpha_1) p(\alpha_2) p(\beta) p(\kappa). \tag{28}$$

Eventually, the relaxed-ELBO can be expressed as

$$\begin{aligned} \tilde{L}(q, \boldsymbol{\Theta}) &= \int q(\boldsymbol{\theta}) \ln \frac{G(\boldsymbol{y}, \boldsymbol{\theta}, \boldsymbol{\Theta})}{q(\boldsymbol{\theta})} d\boldsymbol{\theta} \\ &= \int q(\boldsymbol{\theta}) \ln \frac{G(\boldsymbol{y}, \boldsymbol{\theta}, \boldsymbol{\Theta}) g\boldsymbol{\Theta}}{q(\boldsymbol{\theta}) g(\boldsymbol{\Theta})} d\boldsymbol{\theta} \\ &= \int q(\boldsymbol{\theta}) \ln \frac{\tilde{G}(\boldsymbol{y}, \boldsymbol{\theta}, \boldsymbol{\Theta})}{q(\boldsymbol{\theta})} d\boldsymbol{\theta} - \ln\, g(\boldsymbol{\Theta}) \end{aligned} \tag{29}$$

where $\tilde{G}(\boldsymbol{y}, \boldsymbol{\theta}, \boldsymbol{\Theta}) = G(\boldsymbol{y}, \boldsymbol{\theta}, \boldsymbol{\Theta}) g(\boldsymbol{\Theta})$ with normalizing term

$$g(\boldsymbol{\Theta}) = \frac{1}{\int G(\boldsymbol{y}, \boldsymbol{\theta}, \boldsymbol{\Theta}) d\boldsymbol{\theta} d\boldsymbol{y}}. \tag{30}$$

Because $q(\boldsymbol{\theta}) = q(\boldsymbol{x})q(\alpha_1)q(\alpha_2)q(\beta)q(\kappa)$, the primary aim was to maximize $\tilde{L}(q, \Theta)$ with respect to $q(\boldsymbol{x})$, $q(\alpha_1)q(\alpha_2)$, $q(\beta)$, $q(\kappa)$, and parameter z. In the E-step, the lower bound $\tilde{L}(q, \Theta)$ is maximized with respect to $q(\boldsymbol{\theta})$ in order to evaluate

$q^{\text{new}}(\boldsymbol{\theta})$. In other words, the posterior distributions are obtained for each hidden variable, while keeping the rest of the variables fixed. Whereas, in the subsequent maximization step (M-step), $q(\theta)$ is held fixed and $\tilde{L}(q^{\text{new}}, \boldsymbol{\Theta})$ is maximized with respect to the parameter $\boldsymbol{\Theta}$ to evaluate a new parameter estimate $\boldsymbol{\Theta}^{\text{new}}$. The detailed explanation of the Bayesian inference is given below.

3.1.2 | E-step

Update of $q(\boldsymbol{x})$: Excluding those terms that are independent of $\boldsymbol{x}$, the approximate posterior distribution can be obtained as

$$\begin{aligned}
&\ln q(\boldsymbol{x}) \propto \langle \ln \tilde{G}(\boldsymbol{y},\boldsymbol{\theta},z)\rangle_{q(\alpha_1)q(\alpha_2)q(\beta)q(\kappa)} + \text{constant}\\
&\propto \langle \ln F(\boldsymbol{y},\boldsymbol{x},z,\beta) + \ln p(\boldsymbol{x}|\alpha_1,\alpha_2,\kappa;v)\rangle_{q(\alpha_1)q(\alpha_2)q(\beta)q(\kappa)} + \text{const.}\\
&\propto \ln F(\boldsymbol{y},\boldsymbol{x},z,\beta)\\
&-\frac{1}{2}\sum_{i=1}^{K}\left[\langle\alpha_{i1}\rangle\langle\kappa_i\rangle(x_i-v)^2 + \langle\alpha_{i2}\rangle\langle 1-\kappa_i\rangle(x_i+v)^2\right] + \text{const.}\\
&\propto -\boldsymbol{x}^{\mathrm{H}}\left[\langle\beta\rangle\frac{T}{2}\mathbf{I} + \mathbf{D}_1 + \mathbf{D}_2\right]\boldsymbol{x}\\
&+2\boldsymbol{x}^{\mathrm{H}}\left(\langle\beta\rangle\left(\mathbf{H}^{\mathrm{H}}\mathbf{H}\boldsymbol{z} - \mathbf{H}^{\mathrm{H}} - \frac{T}{2}z\right) - v(\mathbf{A_1} - \mathbf{A}_2)\right) + \text{constant}\\
&\propto -\boldsymbol{x}^{\mathrm{H}}\sum{}^{-1}\boldsymbol{x} + 2\boldsymbol{x}^{\mathrm{H}}\sum{}^{-1}\mu + \text{constant}
\end{aligned} \tag{31}$$

where

$$\begin{aligned}
\mathbf{D}_1 &= \text{diag}(\langle\alpha_{i1}\rangle\langle\kappa_i\rangle, \ldots\ldots\ldots, \langle\alpha_{K1}\rangle\langle\kappa_K\rangle),\\
\mathbf{D}_2 &= \text{diag}(\langle\alpha_{i2}\rangle\langle 1-\kappa_i\rangle, \ldots\ldots\ldots, \langle\alpha_{K2}\rangle\langle 1-\kappa_K\rangle)
\end{aligned} \tag{32}$$

and

$$\begin{aligned}
\mathbf{A}_1 &= (\langle\alpha_{i1}\rangle\langle\kappa_i\rangle, \ldots\ldots\ldots, \langle\alpha_{K1}\rangle\langle\kappa_K\rangle),\\
\mathbf{A}_2 &= (\langle\alpha_{i2}\rangle\langle 1-\kappa_i\rangle, \ldots\ldots\ldots, \langle\alpha_{K2}\rangle\langle 1-\kappa_K\rangle)
\end{aligned} \tag{33}$$

Clearly, this is the exponent of a Gaussian distribution with its mean μ and covariance matrix Σ given by

$$\mu = \sum\left(\langle\beta\rangle\left(\mathbf{H}^{\mathrm{H}}\mathbf{H}\boldsymbol{z} - \mathbf{H}^{\mathrm{H}}\boldsymbol{y} - \frac{T}{2}z\right) - v(\mathbf{A}_1 - \mathbf{A}_2)\right), \tag{34}$$

$$\sum = \left[\langle\beta\rangle\frac{T}{2}\mathbf{I} + \mathbf{D}_1 + \mathbf{D}_2\right]^{-1}. \tag{35}$$

Thus, $a(\boldsymbol{x})$ has the following truncated Gaussian form

$$q(\boldsymbol{x_i}) = \begin{cases} \frac{\mathrm{N}(x_i|\mu_i,\sum_{i,i})}{\phi_i} & \text{if } \boldsymbol{x_i} \in [-v, v],\\ 0 & \text{otherwise} \end{cases} \tag{36}$$

where the normalization constant $\varphi_{\boldsymbol{i}}$ is given as

$$\phi_{\boldsymbol{i}} = \varphi\left(\frac{v-\mu_{\boldsymbol{i}}}{\text{sqrt}(\sum_{i,i})}\right) - \varphi\left(\frac{-v-\mu_{\boldsymbol{i}}}{\text{sqrt}(\sum_{i,i})}\right). \tag{37}$$

Update of $q(\alpha_1)$*:* Retaining those terms that are dependent on α_1, the approximate posterior $q(\alpha_1)$ can be obtained as

$$\begin{aligned}
&\ln q(\alpha_1)\\
&\propto \langle \ln \tilde{G}(\boldsymbol{y},\boldsymbol{\theta},z)\rangle_{q(\boldsymbol{x})q(\alpha_2)q(\beta)q(\kappa)} + \text{constant}\\
&\propto \langle \ln p(\boldsymbol{x}|\alpha_1,\alpha_2,\kappa;v) + \ln p(\alpha_1;a,b)\rangle_{q(\boldsymbol{x})q(\alpha_2)q(\beta)q(\kappa)} + \text{const.}\\
&\propto \frac{1}{2}\langle\kappa_i\rangle\sum_{i=1}^{K}\ln\alpha_{i1} - \sum_{i=1}^{K}\langle\kappa_i\rangle\ln\eta_{i1} - \frac{1}{2}\sum_{i=1}^{K}\left\langle(\boldsymbol{x}_i - v)^2\right\rangle\langle\kappa_i\rangle\alpha_{i1}\\
&\quad + (a-1)\sum_{i=1}^{K}\ln\alpha_{i1} - b\sum_{i=1}^{K}\alpha_{i1} + \text{constant}\\
&\propto -\sum_{i=1}^{K}\langle\kappa_i\rangle\ln\eta_{i1} - \sum_{i=1}^{K}\left(\left(a + \frac{1}{2}\langle\kappa_i\rangle - 1\right)\ln\alpha_{i1}\right)\\
&\quad - \left(b + \frac{1}{2}\langle\kappa_i\rangle\left\langle(\boldsymbol{x}_i - v)^2\right\rangle\right)\alpha_{i1} + \text{constant}.
\end{aligned} \tag{38}$$

Notice that $\ln q(\alpha_1)$ has factorized form $\ln q(\alpha_1) = \Sigma_{\boldsymbol{i}}\ln q(\alpha_{i1})$. Using the approximations adopted in [30], we arrive at

$$\begin{aligned}
&\ln q(\alpha_1)\\
&\propto \left(\boldsymbol{a} + \frac{1}{2}\langle\kappa\rangle - 1\right)\ln\alpha_{i1} - \left(\boldsymbol{b} + \frac{1}{2}\langle\kappa_i\rangle\left\langle(\boldsymbol{x}_i - v)^2\right\rangle\right)\alpha_{i1} + \text{const.}
\end{aligned} \tag{39}$$

Thus, α_1 obeys a Gamma distribution

$$q(\alpha_{i1}) = \text{Gamma}(\alpha_{i1}; \tilde{\boldsymbol{a}}_{i1}, \tilde{\boldsymbol{b}}_{i1}) \tag{40}$$

with the parameters $\tilde{\boldsymbol{a}}_{i1}$ and $\tilde{\boldsymbol{b}}_{i1}$ are, respectively, given as

$$\tilde{\boldsymbol{a}}_{i1} = \boldsymbol{a} + \frac{1}{2}\langle\kappa_i\rangle \tag{41a}$$

and

$$\tilde{\boldsymbol{b}}_{i1} = \boldsymbol{b} + \frac{1}{2}\langle\kappa_i\rangle\left\langle(x_i - v)^2\right\rangle \tag{41b}$$

By symmetry, the posterior $q(\alpha_2)$ can be obtained as

$$q(\alpha_{i2}) = \text{Gamma}(\alpha_{i2}; \tilde{\boldsymbol{a}}_{i2}, \tilde{\boldsymbol{b}}_{i2}) \tag{42}$$

with the parameters $\tilde{\boldsymbol{a}}_{i2}$ and $\tilde{\boldsymbol{b}}_{i2}$ are, respectively, given as

$$\tilde{\boldsymbol{a}}_{i2} = \boldsymbol{a} + \frac{1}{2}(1 - \langle\kappa_i\rangle) \tag{43a}$$

and

$$\tilde{\boldsymbol{b}}_{i2} = b + \frac{1}{2}(1 - \langle\kappa_{\boldsymbol{i}}\rangle)\left\langle(x_i + v)^2\right\rangle. \tag{43b}$$

Update of $q(\kappa)$: The variational optimization of $q(\kappa)$ can be obtained as

$$\begin{aligned}
\ln q(\kappa) &\propto \langle \ln p(\boldsymbol{y},\boldsymbol{x},\alpha_1,\alpha_2,\kappa,\beta;v)\rangle_{q(\boldsymbol{x})q(\alpha_1)q(\alpha_2)q(\beta)} + \text{constant}\\
&\propto \langle \ln p(\boldsymbol{x}|\alpha_1,\alpha_2,\kappa;v) + \ln p(k)\rangle_{q(\boldsymbol{x})q(\alpha_1)q(\alpha_2)q(\beta)} + \text{constant}\\
&\propto \sum_{i=1}^{K}\left(\frac{1}{2}\left(\langle\ln\alpha_{i1}\rangle - \langle\ln\alpha_{i2}\rangle - \left\langle(x_i - v)^2\right\rangle\right.\right.\\
&\quad \left.\left. + \left\langle(x_i + v)^2\right\rangle\right)\right)\kappa_i + \sum_{i=1}^{K}\left(\langle\ln\eta_{i2} - \langle\ln\eta_{i1}\rangle\rangle\right.\\
&\quad \left. + \ln\frac{\pi}{1-\pi}\right)\kappa_i + \text{const.}
\end{aligned} \tag{44}$$

Update of $q(\beta)$: Finally, the posterior distribution of noise variance can be obtained as

$$\begin{aligned}\ln q(\beta) &\propto \langle \ln \tilde{G}(\boldsymbol{y},\boldsymbol{\theta},z)\rangle_{q(\boldsymbol{x})q(\alpha_1)q(\alpha_2)q(\kappa)} + \text{constant} \\ &\propto \langle \ln F(\boldsymbol{y},\boldsymbol{x},\boldsymbol{z},\beta) + \ln p(\beta;c,d)\rangle_{q(\boldsymbol{x})q(\alpha_1)q(\alpha_2)q(\kappa)} + \text{const.} \\ &\propto \left(\boldsymbol{c} - 1 + \frac{J}{2}\ln\beta - \frac{1}{2}\langle \boldsymbol{g}(\boldsymbol{x},\boldsymbol{z})\rangle + \boldsymbol{d}\right)\beta + \text{const.}\end{aligned} \tag{45}$$

Therefore, β obeys a Gamma distribution

$$q(\beta) = \text{Gamma}(\beta;\tilde{\boldsymbol{c}},\tilde{\boldsymbol{d}}). \tag{46}$$

With the parameters $\tilde{\boldsymbol{c}}$ and $\tilde{\boldsymbol{d}}$ given as

$$\tilde{\boldsymbol{c}} = \boldsymbol{c} + \frac{J}{2} \tag{47a}$$

and

$$\tilde{\boldsymbol{d}} = \frac{1}{2}\langle g(\boldsymbol{x},\boldsymbol{z})\rangle + \boldsymbol{d} \tag{47b}$$

Conclusively, the E-step successively computes the approximate posterior distribution for each hidden variable. The expectations and moments employed during the update can be summarized as follows:

$$\langle \boldsymbol{x}_i^2\rangle = \mu_i^2 + \sum_{i,i} - \frac{\sum_{i,i}}{\phi_i}\left(\text{N}\left(\upsilon|\mu_i,\sum_{i,i}\right) + \text{N}\left(-\upsilon|\mu_i,\sum_{i,i}\right)\right), \tag{48}$$

$$\langle \alpha_{il}\rangle = \tilde{\boldsymbol{a}}_{il}/\tilde{\boldsymbol{b}}_{il}, l = 1,2, \tag{49}$$

$$\langle \kappa_i\rangle = q(\kappa_i = 1), \tag{50}$$

$$\begin{aligned}\langle g(\boldsymbol{x},\boldsymbol{z})\rangle &= \|\boldsymbol{y} - \mathbf{H}\boldsymbol{z}\|_2^2 + 2(\mu - z)^{\text{T}}\mathbf{H}^T(\mathbf{H}\boldsymbol{z} - \boldsymbol{y}) \\ &+ \frac{T}{2}\left(\|\mu - z\|_2^2 + \text{Tr}(\sum)\right)\end{aligned} \tag{51}$$

3.1.3 | M-step

As previously mentioned, in the M-step, the complete log-likelihood is maximized in order to obtain the deterministic parameters $\Theta = \{v, z\}$, that is,

$$\Theta^{\text{new}} = \arg\max_{\Theta}\langle \ln\, G(\boldsymbol{y},\theta;\Theta)\rangle_{\boldsymbol{q}(\Theta)} = \boldsymbol{Q}(\Theta,\Theta^{\textbf{old}}). \tag{52}$$

Update of parameter z: The update of the parameter $\boldsymbol{z}$ is obtained by maximizing the complete likelihood $\boldsymbol{Q}(z, z^{\text{old}})$ with respect to $\boldsymbol{z}$:

$$\boldsymbol{Q}\left(z|z^{\text{old}}\right) = z^{\text{new}} = \arg\max_{z}\langle \ln\, G(\boldsymbol{y},\theta,\boldsymbol{z})\rangle_{q(\theta;z^{\text{old}})}. \tag{53}$$

Setting its derivative to zero yields:

$$\frac{\partial \boldsymbol{Q}\left(z|z^{\text{old}}\right)}{\partial z} = \left\langle (T\mathbf{I} - 2\mathbf{H}^{\text{H}}\mathbf{H})(z - \boldsymbol{x})\right\rangle_{q(\theta;z^{\text{old}})} = 0 \Rightarrow \boldsymbol{z} = \mu. \tag{54}$$

Update of parameter v: In the same manner, we can obtain the boundary parameter v by maximizing the complete log-likelihood function $\boldsymbol{Q}$ with respect to v. We adopted the heuristic approach from [25] to update v, where the parameter v is increased so as to reduce the mismatch $\delta(\hat{x}) = \|y - H\hat{x}\|_2^2$.

Here, the estimated signal $\hat{\boldsymbol{x}}$ denotes the mean of the posterior distribution $q(\boldsymbol{x})$. Motivated by [25], the step size Δv is given by

$$\Delta v = \frac{(\boldsymbol{y} - \mathbf{H}\hat{\boldsymbol{x}}^{(t)})^{\text{T}}\mathbf{H}\gamma}{\|\mathbf{H}\gamma\|_2^2}\delta(\hat{\boldsymbol{x}}) = \|\boldsymbol{y} - \mathbf{H}\hat{\boldsymbol{x}}\|_2^2. \tag{55}$$

At iteration t,

$$\gamma_i = \begin{cases} 1, & \text{if } \hat{\boldsymbol{x}}_i^{(t)} \geq 0 \\ -1, & \text{if } \hat{\boldsymbol{x}}_i^{(t)} < 0 \end{cases}. \tag{56}$$

Eventually, the update for the parameter v can be obtained as

$$\boldsymbol{v}^{\boldsymbol{t+1}} = v^t + \Delta v. \tag{57}$$

For clarity, the key steps of the variational Bayesian method are summarized as follows:

Key steps of variational Bayesian method
Initialization: Let iteration count t = 0. Initialize the means of posteriors $q(\boldsymbol{x})$, $q(\alpha_1)$, $q(\alpha_2)$, $q(\kappa)$ as 0, 1, 1, and 0.5, respectively, and the variance of $q(\boldsymbol{x})$ as 1.
Repeat the following steps until $t \geq t_{\text{MAX}}$
Step 1: Given the current estimate of z, obtain the updated posteriors of hidden variables: $q(\boldsymbol{x})$, $q(\alpha_1)$, $q(\alpha_2)$, $q(\kappa)$ and $q(\beta)$ according to (34)–(35), (40), (42), (44), and (46).
Step 2: Obtain the new estimate v^{t+1} using (55)–(57) and update the parameter z according to (54).
Step 3: Set $t \rightarrow t + 1$ and return to step 1.

3.2 | Computational complexity analysis

The update of $q(\boldsymbol{x})$ involves a $K \times K$ inverse operation, but the matrix to be inverted [c.f., (35)] is now a diagonal matrix. Hence, the computational complexity is significantly reduced when compared to conventional SBL [19], which scales as (K^3). Evidently, the proposed algorithm is free of any matrix-inverse operations, and the dominating operations in each iteration only involve simple matrix-vector multiplications, which scale as $\mathcal{O}(J, K)$ $(J < K)$. Moreover, the update of other hidden variables α_1, α_2, β, and the parameter $\boldsymbol{z}$ also involves simple addition and multiplication operations.

4 | SIMULATION RESULTS

In this section, we demonstrate the PAPR reduction performance of the proposed truncated Gaussian mixture (TGM) model based inverse-free SBL method (referred to as the IF-TGM-SBL). In addition to our proposed method, we also consider the performance of FITRA [15], variational EM-GAMP algorithm [25], and the conventional ZF precoding scheme for 1,000 independent trials. In all of the simulations, we set $a = b = c = d = 10^{-10}$, and $\boldsymbol{T}$ is selected to be slightly larger than the (smallest) Lipschitz constant, that is, $\boldsymbol{T} = 2\lambda_{\max}(\mathbf{H}^{\mathrm{H}}\mathbf{H})$, where $\lambda_{\max}$ denotes the maximum eigenvalue. As indicated in [15], the regularization parameter λ for FITRA is set to be 0.25. The simulations were carried out for a massive MIMO downlink scenario having $N = 100$ transmit antennas and 10 single-antenna user terminals. OFDM modulation with $U = 128$ tones and spectral map Γ with 114 data carrying tones were considered as specified in the 40-MHz mode of IEEE802.11n [31]. For simulation purposes, coded transmission was employed, that is, the information bits for each user are encoded by a convolutional encoder (rate-1/2, generator polynomials $[133_0,171_0]$ and constraint length 7), which are then interleaved, mapped to 16-QAM constellation using Gray labeling, precoded, and finally transmitted over the assumed frequency-selective channel. The channel is modeled as a tap-delay line with $R = 4$ taps, and impulse response matrices $\hat{\mathbf{H}}_r, r = 1, \ldots, R$, have i.i.d. entries drawn from a circularly symmetric standard Gaussian distribution. The frequency-domain response $\mathbf{H}_u$ on the uth tone can be expressed as:

$$\mathbf{H}_u = \sum_{r=1}^{R} \hat{\mathbf{H}}_r \exp\left(\frac{-j2\pi \mathrm{du}}{U}\right). \tag{58}$$

After demodulation at each user terminal, a soft-input Viterbi decoder is used to regenerate the transmitted bits.

In the simulations, the probability of PAPR exceeding a threshold PAPR_0 is considered as the measurement index, and is described as the complementary cumulative distribution function (CCDF) [32].

$$\mathrm{CCDF}(\mathrm{PAPR}_0) = \Pr(\mathrm{PAPR} > \mathrm{PAPR}_0). \tag{59}$$

In addition, in order to evaluate the out-of-band radiation of the solution, we define the out-of-band (power) ratio (OBR) as:

$$\mathrm{OBR} = \frac{|\Gamma| \sum_{u \in \Gamma^c} \|\boldsymbol{p}_u\|_2^2}{|\Gamma^C| \sum_{u \in \Gamma} \|\boldsymbol{p}_u\|_2^2}. \tag{60}$$

To investigate the PAPR reduction performance, Figure 3 shows a comparison of the complementary CDF of the PAPR values for all considered schemes obtained in 1,000 simulation trials in. The PAPR values associated with all N transmit antennas are considered while calculating the empirical CCDF. For a system configuration with $(N, M) = (100, 10)$, the IF-TGM-SBL algorithm, within 500 iterations, is able to reduce the PAPR by 0.8 dB (corresponding to a complementary CDF of 10^{-4}) compared to the FITRA algorithm at $\lambda = 0.25$, which needs to perform 2,000 iterations. Moreover, a reduction of 11.5 dB in the PAPR is obtained when compared to the ZF scheme. Among the considered algorithms, EM-GAMP with 200 iterations can obtain a PAPR that is even lower than IF-TGM-SBL, but this is at the expense of an increased SNR loss. It can be observed that the PAPR reduction performance of FITRA is susceptible to the choice of the regularization parameter λ, whereas IF-TGM-SBL is free of this issue. Meanwhile, IF-TGM-SBL exhibits a much lower OBR (averaged over 1,000 independent runs) than the FITRA algorithm. For $\lambda = 2^j$ with $j \in \{-2, -3, -4\}$, FITRA attains OBR values of -56.18 dB, -58.95 dB, and -61.11 dB, respectively, whereas IF-TGM-SBL renders an OBR value of -66.91 dB. Thus, at $\lambda = 2^{-4}$, the lowest OBR value is attained by FITRA, but at the cost of a significant increase in the PAPR.

The symbol error rate (SER) performance of all considered algorithms is depicted in Figure 4. The average signal-to-noise ratio (SNR) across user terminals is defined as $\|\boldsymbol{x}\|_2^2/\boldsymbol{N}\boldsymbol{N_o}$ where $\boldsymbol{N_o}$ denotes the noise variance at the receivers. At SER of 10^{-4}, we observe that the IF-TGM-SBL incurs a SNR loss of about 1.75 dB and 0.3 dB compared to ZF precoding and FITRA algorithm (at $\lambda = 0.25$), respectively, whereas outperforms EM-GAMP by about 0.45 dB. As discussed in [15], the SNR performance loss occurs because the norm of the solution obtained by our proposed method has a more significant increase than FITRA algorithm. Among the considered schemes, ZF precoding attains the least-norm solution. In Figures 3 and 4, we can also observe that increasing regularization parameter λ for FITRA reduces the PAPR but degrades the SNR operating point.

We now examine the convergence behavior of FITRA (at regularization parameter $\lambda = 0.25$), EM-GAMP, and our proposed algorithm for system configuration $(N, M) = (100, 10)$. Figure 5 plots the PAPR performance of these algorithms as a function of the number of iterations. It can be observed that IF-TGM-SBL yields a much faster convergence rate than the

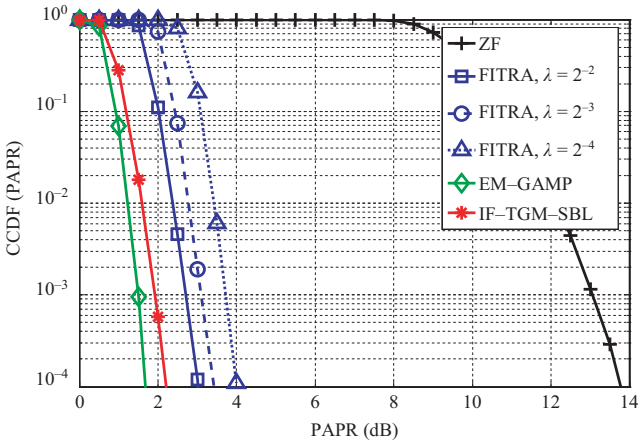

FIGURE 3 PAPR performance for different schemes for $(N, M) = (100,10)$

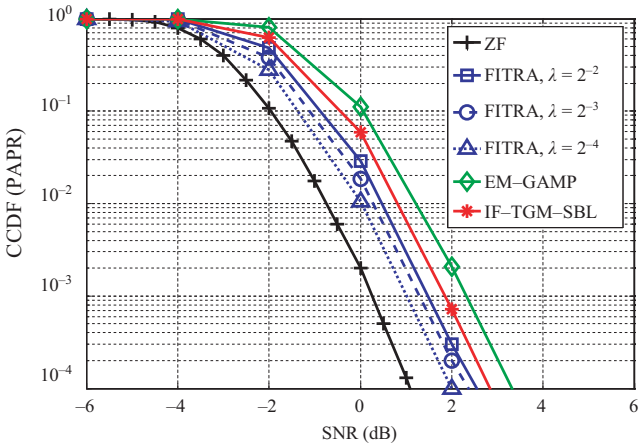

FIGURE 4 SER performance for the considered schemes

FITRA algorithm, because the former converges to a low-PAPR value within only ~450 iterations, whereas the latter performs about 2,000 iterations to obtain a fairly low-PAPR solution. We observe that the IF-TGM-SBL algorithm can obtain a PAPR of 4 dB within only ~50 iterations, while the FITRA algorithm requires as many as 1,000 iterations to obtain a similar result. We also note that IF-TGM-SBL shows comparable convergence rate with the EM-GAMP method, although the latter achieves comparably lower PAPR values.

To investigate the impact of the transmit antenna configuration on the PAPR reduction, we now examine the PAPR results averaged over 1,000 independent trials as a function of the number of BS antennas N for a fixed number of user terminals $M = 10$. From Figure 6, it is evident that increasing the number of transmit antennas from 20 to 100 yields improved PAPR performance for all of the considered algorithms. This is expected because increasing the number of transmit antennas will result in an increase in the number of DoFs at the BS. Both the Bayesian methods, that is, IF-TGM-SBL and EM-GAMP, perform notably better compared with

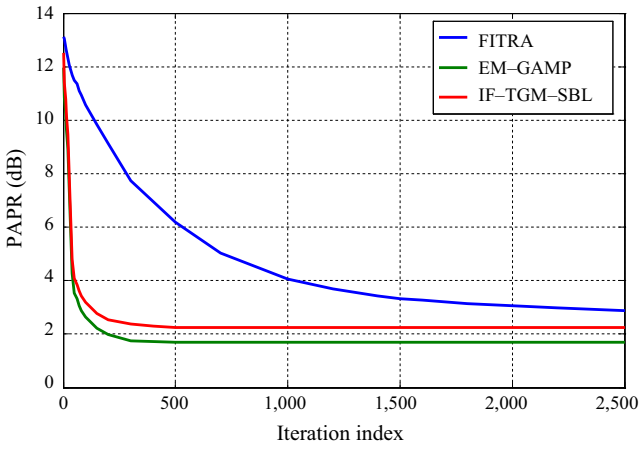

FIGURE 5 Comparison of the convergence rates of the PAPR metric for FITRA and IF-TGM-SBL algorithms for $(N, M) = (100, 10)$

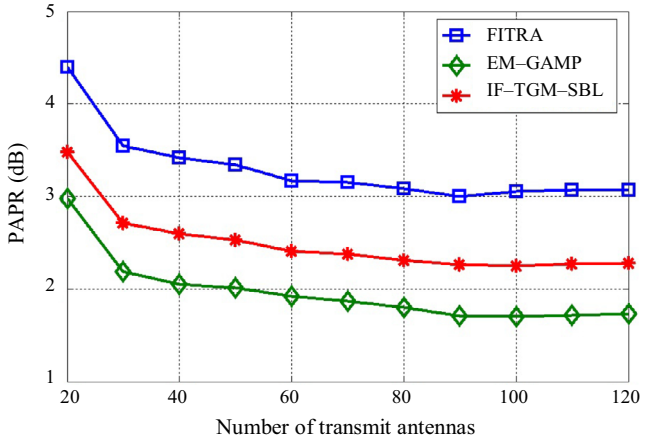

FIGURE 6 PAPR performance of FITRA and IF-TGM-SBL algorithms vs. number of transmit antennas for $M = 10$ and regularization parameter $\lambda = 0.25$ for FITRA

the FITRA scheme in terms of exploiting the inherent DoFs as the number of transmit antennas increases. Based on a detailed inspection, the proposed method offers a reduction of about 0.74 dB and 0.79 PAPR compared to FITRA, when $(N, M) = (60, 10)$ and $(N, M) = (120, 10)$, respectively.

5 | CONCLUSION

In this paper, we introduced a variant of the sparse Bayesian learning (SBL) method for joint consideration of PAPR reduction and MUI cancellation in massive MIMO-OFDM systems. The proposed method circumvents the matrix-inverse operation involved in the standard SBL method by invoking and maximizing the recently proposed relaxed-ELBO [26] using a variational EM algorithm. The resulting inverse-free Bayesian approach exhibits an optimal rate of convergence for the PAPR metric in terms of its dependence on the number of iterations. Simulation results show that the proposed method efficiently exploits the large DoFs inherent in large-scale antenna systems in order to obtain lower PAPRs than the existing methods, while producing lower out-of-band radiation.

ORCID

Davinder Singh https://orcid.org/0000-0002-0168-5158

REFERENCES

1. T. L. Marzetta, *Noncooperative cellular wireless with unlimited numbers of base station antennas*, IEEE Trans. Wireless Commun. **9** (2010), no. 11, 3590–3600.
2. B. M. Hochwald, T. L. Marzetta, and V. Tarokh, *Multiple-antenna channel hardening and its implications for rate feedback and scheduling*, IEEE Trans. Info. Theory **50** (2004), no. 9, 1893–1909.

3. L. Lu et al., *Overview of massive MIMO: Benefits and challenges*, IEEE J. Sel. Topics in Sig. Process. **8** (2014), no. 5, 742–758.
4. G. Wunder et al., *The PAPR problem in OFDM transmission: New directions for a long-lasting problem*, IEEE Sig. Process. Mag. **30** (2013), no. 6, 130–144.
5. M. J. Hao and C. H. Lai, *Precoding for PAPR reduction of OFDM signals with minimum error probability*, IEEE Trans. Broadcast. **56** (2010), no. 1, 120–128.
6. L. Wang and C. Tellambura, *A simplified clipping and filtering technique for PAR reduction in OFDM systems*, IEEE Sig. Process. Lett. **12** (2005), no. 6, 453–456.
7. L. Yang et al., *PAPR reduction of an OFDM signal by use of PTS with low computational complexity*, IEEE Trans. Broadcast. **52** (2006), no. 1, 83–86.
8. J. C. Chen, M. H. Chiu, and Y. S. Yang, *A suboptimal tone reservation algorithm based on cross-entropy method for PAPR reduction in OFDM systems*, IEEE Trans. Broadcast. **57** (2011), no. 3, 752–756.
9. J. Yang et al., *A modified selected mapping technique to reduce the peak-to- average power ratio of OFDM signal*, IEEE Trans. Consumer Electr. **53** (2007), no. 3, 846–851.
10. B. S. Krongold and D. L. Jones, *PAR reduction in OFDM via active constellation extension*, IEEE Trans. Broadcast. **49** (2003), no. 3, 258–268.
11. M. Iwasaki and K. Higuchi, Clipping and filtering-based PAPR reduction method for precoded OFDM-MIMO signals, in *Proc. IEEE 71st Veh. Tech. Conf.*, Taipei, Taiwan, 2010, pp. 1–5.
12. E. Manasseh, S. Ohno, and M. Nakamoto, *Combined channel estimation and PAPR reduction technique for MIMO–OFDM systems with null subcarriers*, EURASIP J. Wirel. Commun. Netw. **2012** (2012), no. 1, 1–15.
13. H. B. Jeon, J.-S. No, and D.-J. Shin, *A low-complexity SLM Scheme using additive mapping sequences for PAPR Reduction of OFDM signals*, IEEE Trans. Broadcast. **57** (2011), no. 4, 866–875.
14. S.-J. Ku, *Low-complexity PTS-based schemes for PAPR reduction in SFBC MIMO-OFDM systems*, IEEE Trans. Broadcast. **60** (2014), no. 4, 650–658.
15. C. Studer and E. G. Larsson, *PAR-aware large-scale multi-user MIMO OFDM downlink*, IEEE J. Sel. Areas Commun. **31** (2013), no. 2, 303–313.
16. D. L. Donoho, *Compressed sensing*, IEEE Trans. Inform. Theory **52** (2006), no. 4, 1289–1306.
17. B. Ebrahim et al., *Peak reduction and clipping mitigation in OFDM by augmented compressive sensing*, IEEE Trans. Sig. Process. **60** (2012), no. 7, 3834–3839.
18. B. Liu et al., *A low-complexity compressive sensing algorithm for PAPR reduction*, Wireless Pers. Commun. **78** (2014), no. 1, 283–295.
19. M. E. Tipping, *Sparse Bayesian learning and the relevance vector machine*, J. Mach. Learn. Res **1** (2001), no. 1, 211–244.
20. T. T. Ballen, J. A. Tropp, and A. C. Gilbert, *Signal recovery from random measurements via orthogonal matching pursuit*, IEEE Trans. Inform. Theory **53** (2007), no. 2, 4655–4666.
21. E. J. Candes and T. Tao, *Decoding by linear programming*, IEEE Trans. Inform. Theory **51** (2005), no. 12, 4203–4215.
22. J. P. Vila and P. Schniter, *Expectation-maximization gaussian-mixture approximate message passing*, IEEE Trans. Sig. Process. **61** (2013), no. **19**, 4658–4672.
23. S. Som and P. Schniter, *Compressive imaging using approximate message passing and a Markov-tree prior*, IEEE Trans. Sig. Process. **60** (2012), no. 7, 3439–3448.
24. J. Fang, L. Zhang, and H. Li, *Two-dimensional pattern-coupled sparse Bayesian learning via generalized approximate message passing*, IEEE Trans. Image Process. **25** (2016), no. 6, 2920–2930.
25. H. Bao et al., *An efficient Bayesian PAPR reduction method for OFDM- based massive MIMO systems*, IEEE Trans. Wireless Commun. **15** (2016), no. 6, 4183–4195.
26. H. Duan et al., *Fast inverse-free sparse Bayesian learning via relaxed evidence lower bound maximization*, IEEE Sig. Process. Lett. **24** (2017), no. 6, 774–778.
27. M. Joham, W. Utschick, and J. Nossek, *Linear transmit processing in MIMO communications systems*, IEEE Trans. Sig. Process. **53** (2005), no. 8, 2700–2712.
28. C. Studer et al., *Democratic representations*, ArXiv preprint (2015), arXiv: 1401.3420.
29. D. G. Tzikas, A. C. Likas, and N. P. Galatsanos, *The variational approximation for Bayesian inference*, IEEE Sig. Process. Mag. **25** (2008), no. 6, 131–146.
30. J. P. Vila and P. Schniter, *An empirical-bayes approach to recovering linearly constrained non-negative sparse signals*, IEEE Trans. Sig. Process. **62** (2014), no. 18, 4689–4703.
31. IEEE 802.11 Working Group, *Part 11: Wireless LAN medium access control (MAC) and physical layer (PHY) specifications, amendment 5: Enhancements for higher throughput*, IEEE, 2009.
32. H. Ochiai and H. Imai, *On the distribution of the peak-to-average power ratio in OFDM signals*, IEEE Trans. Commun. **49** (2001), no. 2, 282–289.

AUTHOR BIOGRAPHIES

Davinder Singh received his BTech in electronics and communication engineering (ECE) from the I.K. Gujral Punjab Technical University, Punjab, India, in 2011, his ME in ECE from Panjab University, Chandigarh, India, in 2013, and he is currently working toward the PhD degree at the Dr. B.R. Ambedkar National Institute of Technology, Jalandhar, Punjab, India. His main research interests are signal processing for wireless communication and MIMO wireless systems.

Rakesh Kumar Sarin received his BSc degree in electronics and communication engineering (ECE) from the National Institute of Technology, Kurukshetra, India, in 1978, his ME in ECE from the Indian Institute of Technology, Roorkee, Uttrakhand, India in 1980, and his PhD from A.F. Ioffe Physico Technical Institute, St. Petersburg, Russian 1987. His research interests are in semiconductors, microelectronics/VLSI, RF, and microwaves.